

Improved solid stability from a screened range-separated hybrid functional by satisfying semiclassical atom theory and local density linear response

Subrata Jana,^{1,*} Bikash Patra^{1,†} Szymon Śmiga^{2,‡} Lucian A. Constantin^{3,§} and Prasanjit Samal^{1,||}

¹*School of Physical Sciences, National Institute of Science Education and Research, HBNI, Bhubaneswar 752050, India*

²*Institute of Physics, Faculty of Physics, Astronomy and Informatics, Nicolaus Copernicus University, Grudziadzka 5, 87-100 Toruń, Poland*

³*Istituto di Nanoscienze, Consiglio Nazionale delle Ricerche CNR-NANO, 41125 Modena, Italy*



(Received 14 July 2020; accepted 18 September 2020; published 6 October 2020)

Semiclassical neutral atom theory is an important constraint of the state-of-the-art development of exchange-correlation functionals for solid-state physics. Based on this theory, we construct a screened range-separated hybrid functional for strongly bound bulk solids, which also satisfies the accurate linear response of the local density approximation. The constructed functional shows remarkable performance and is competitive with other popular screened hybrids. Our comprehensive assessment of the constructed screened hybrid for the general purpose solid-state structural properties, structural phase transition, prototypical ferroelectric properties, band gaps, and optical absorption spectra is showing its accuracy for the diverse nature of solid-state properties. Moreover, when applied to general purpose chemical applications, the constructed functional is also reasonably accurate and competitive. Accurate screened hybrids based on semiclassical neutral atom theory are appealing for various solid-state and material science applications and are also attractive for the development of the dielectric-dependent hybrids for interfaces and surfaces.

DOI: [10.1103/PhysRevB.102.155107](https://doi.org/10.1103/PhysRevB.102.155107)

I. INTRODUCTION

The Kohn-Sham (KS) formalism [1] of density functional theory (DFT) [2] is one of the most successful computational tools for the ground-state electronic structure calculations of solids. Due to the development of simple and accurate exchange-correlation (XC) functional approximations [3–5], the KSDFT has achieved a very attractive ratio between the computational time and accuracy. The most effective XC approximations for predicting the equilibrium lattice constants, atomic radii, atomic distances and angles, and bulk moduli of strongly bound bulk solids, are the semilocal XC functionals, which are classified on the first three rungs of the Jacob’s ladder [6–8], in function of their sophistication. Thus, on the first rung lays the local density approximation (LDA) [1], whose XC energy per particle $\epsilon_{xc}^{LDA}[n_{\uparrow}(\mathbf{r}), n_{\downarrow}(\mathbf{r})]$ depends only on the spin-densities $n_{\uparrow}(\mathbf{r})$, and $n_{\downarrow}(\mathbf{r})$. (We recall that ϵ_{xc} is defined by $E_{xc} = \int d\mathbf{r} n \epsilon_{xc}$.) The next rungs are represented by generalized gradient approximations (GGAs) that depends on gradients of spin densities $\epsilon_{xc}^{GGA}[n_{\uparrow}(\mathbf{r}), n_{\downarrow}(\mathbf{r}), \nabla n_{\uparrow}(\mathbf{r}), \nabla n_{\downarrow}(\mathbf{r})]$, and meta-GGAs which use as additional ingredients the spin-dependent kinetic energy densities τ_{\uparrow} and τ_{\downarrow} , such that $\epsilon_{xc}^{MGGGA}[n_{\uparrow}(\mathbf{r}), n_{\downarrow}(\mathbf{r}), \nabla n_{\uparrow}(\mathbf{r}), \nabla n_{\downarrow}(\mathbf{r}), \tau_{\uparrow}(\mathbf{r}), \tau_{\downarrow}(\mathbf{r})]$.

Nonempirical meta-GGAs [4,9–18] have been constructed to satisfy many exact conditions [19], being usually accurate for ordinarily extended [16] and finite systems [20], and recognizing various types of interactions [21], but because of their dependence on τ_{\uparrow} and τ_{\downarrow} , they are often used in the generalized KSDFT scheme, considering their nonlocal, orbital-dependent XC potential [22]. However, the nonempirical GGAs are much simpler, being usually specialized on a given property or class of systems. Thus, there are several GGA functionals accurate for equilibrium structure of strongly bound bulk solids [23–28]. Between them, we focus, in this article, on the SG4 GGA [28] that recovers the modified fourth-order gradient expansion (MGE4) of the exchange energy

$$\epsilon_x^{MGE4} = \epsilon_x^{LDA} (1 + \mu^{MGE2} s^2 + \mu^{MGE4} s^4), \quad (1)$$

derived from the semiclassical neutral atom with an infinity number of electrons [29,30]. The second- and fourth-order coefficients are $\mu^{MGE2} = 0.26$ and $\mu^{MGE4} = -0.195$, respectively. Here $s = |\nabla n|/[2(3\pi^2)^{1/3}n^{4/3}]$ is the well-known reduced gradient of the density, which is invariant under the uniform density scaling [31,32]. Note that, while the regular GE4 is dependent on the Laplacian of the density $\nabla^2 n$ being fulfilled only by meta-GGAs, the simple MGE4 can be used in the development of any semilocal functional.

In spite of their accuracy, the semilocal XC approximations do not incorporate important physics of many-body systems such as the many electron self interaction problem [33–37] and the ultranonlocality [38–40], which are essential for the excitation energies, exciton, and optical properties of electronic systems. The traditional way to improve the overall functional performance, including these difficult properties,

*subrata.jana@niser.ac.in, subrata.niser@gmail.com

†bikash.patra@niser.ac.in

‡szsmiga@fizyka.umk.pl

§lucian.constantin.68@gmail.com

||psamal@niser.ac.in

is to mix the nonlocal Hartree-Fock (HF) with the semilocal exchange, resulting the hybrid functional [41–66].

The most efficient and used hybrid functionals in solid-state calculations are the short-range (SR) screened hybrids [44], which combine the SR HF exchange with the long-range (LR) semilocal exchange, using usually the following decomposition of the Coulomb operator [67–75]

$$\frac{1}{|\mathbf{r} - \mathbf{r}'|} = w_{ee}^{\text{SR},\omega} + w_{ee}^{\text{LR},\omega} \\ = \underbrace{\frac{\text{Erfc}(\omega|\mathbf{r} - \mathbf{r}'|)}{|\mathbf{r} - \mathbf{r}'|}}_{\text{SR}} + \underbrace{\frac{\text{Erf}(\omega|\mathbf{r} - \mathbf{r}'|)}{|\mathbf{r} - \mathbf{r}'|}}_{\text{LR}}, \quad (2)$$

where ω is the range-separation parameter. We recall that the Coulomb operator can be splitted using various methods [57,76], but the error function (Erf) is the most used. Thus, the ω -dependent SR and LR exchange functionals are defined as $E_x^{\text{SR},\omega} = \frac{1}{2} \int d\mathbf{r} n(\mathbf{r}) \int d\mathbf{u} \frac{1 - \text{Erf}(\omega u)}{u} n_x(\mathbf{r}, \mathbf{r} + \mathbf{u})$ and $E_x^{\text{LR},\omega} = \frac{1}{2} \int d\mathbf{r} n(\mathbf{r}) \int d\mathbf{u} \frac{\text{Erf}(\omega u)}{u} n_x(\mathbf{r}, \mathbf{r} + \mathbf{u})$, where $n_x(\mathbf{r}, \mathbf{r} + \mathbf{u})$ is the exchange hole at position $\mathbf{r} + \mathbf{u}$ around an electron at \mathbf{r} . Therefore, the knowledge of the HF and semilocal exchange holes is required to develop screened hybrid functionals. While the HF exchange hole is well known in terms of the occupied one-particle orbitals $\phi_i \{n_x^{\text{HF}}(\mathbf{r}, \hat{\mathbf{r}}) = -[\sum_i^{\text{occ}} \phi_i^*(\mathbf{r})\phi_i(\hat{\mathbf{r}})]^2 / [2n(\mathbf{r})]\}$, the semilocal exchange hole can be constructed using several techniques, such as Taylor series expansion [77], density matrix expansion [11] or reverse engineered methods [61,75,78]. The most used is the reverse engineered technique where the semilocal exchange functional is reversed in order to construct its underlying exchange hole. In general, a dimensionless exchange hole shape function $\mathcal{J}^{\text{GGA}}(s, y)$ is used to construct the exchange hole model as, $n_x(\mathbf{r}, \mathbf{r} + \mathbf{u}) = n(\mathbf{r})\mathcal{J}^{\text{GGA}}(s, y)$, where $y = k_F u$ and $k_F = (3\pi^2 n)^{1/3}$ is the Fermi wave vector. The construction of the $\mathcal{J}^{\text{GGA}}(s, y)$ is based on the recovery of exact constraints [61,75,78,79], and it has been used for the development of the screened hybrids for solids, such as the popular HSE [44], HSEsol [80], and HSEint [81], based on the PBE GGA [82], PBEsol GGA [23], and PBEint GGA [66,83] functionals, respectively.

In this paper, we develop the SR screened hybrid of the SG4 GGA named SRhSG4, whose correlation functional has been modified from SG4 correlation, such that the entire functional will recover the accurate LDA linear response, which is an important condition for solid-state systems, fulfilled by various functionals, from GGAs [23,28], to meta-GGAs [9], and global [63] and LR-screened hybrids [48]. We recall that the LDA linear response behavior can be approached by XC functionals if the second-order term of the XC gradient expansion vanishes. The constructed SRhSG4 functional performs remarkably for both strongly bound bulk solids and localized systems. The performance of the present functional shows its great accuracy for the solid-state lattice constants, bulk moduli, cohesive energies, the magnetic properties, properties of the prototype ferroelectric, structural phase transition, band gaps, and optical absorption spectra. It performs better than the semilocal SG4 functional and overall more accurate than the hybrids based on the PBE and PBEsol. We also study the

XC multiplicative potentials, computed using the optimized effective potential (OEP) method [84,85].

The present paper is organized as follows. In Sec. II we will briefly overview the SG4 GGA functional and the reverse engineered SG4 exchange hole, and we present the development of SRhSG4 XC functional. We also discuss the SRhSG4 correlation potential computed by the OEP method, and we test the SRhSG4 for the Hooke's atom model system. In Sec. III, we perform a careful assessment of the SRhSG4 for various solid-state properties (equilibrium lattice constants, bulk moduli, cohesive energies, magnetic properties of Fe, Co, and Ni, structural phase transition of Si and Zr, ferroelectric properties, band gaps, and optical properties), and we also show the SRhSG4 performance for small molecules. Last, in Sec. IV we provide our conclusions and discuss future prospects of the functional.

II. THEORY

A. Short review of SG4 GGA functional

The SG4 exchange functional has been constructed to recover the MGE4 of Eq. (1), to satisfy the Lieb-Oxford bound [86–88], and to give the exact exchange ionization potential of the nonrelativistic noble atom with an infinity number of electrons [89]. The SG4 exchange enhancement factor, defined by $\epsilon_x^{\text{SG4}} = \epsilon_x^{\text{LDA}} F_x(s)$, has the following expression [28]

$$F_x = 1 + \kappa_1 + \kappa_2 - \frac{\kappa_1 \left(1 - \frac{\mu_1 s^2}{\kappa_1}\right)}{1 - \left(\frac{\mu_1 s^2}{\kappa_1}\right)^5} - \frac{\kappa_2}{1 + \frac{\mu_2 s^2}{\kappa_2}}, \quad (3)$$

where $\kappa_1=0.5603$, $\kappa_2 = 0.2437$, $\mu_1 = 0.042$, and $\mu_2 = 0.218$.

The SG4 correlation energy per particle is [28]

$$\epsilon_c^{\text{SG4}} = \epsilon_c^{\text{LDA}} + \phi^{\alpha t^3} H(r_s, \zeta, t), \quad (4)$$

where $t = |\nabla n|/[2k_s \phi n]$ is the reduced gradient for correlation, with $k_s = (4k_F/\pi)^{1/2}$ being the Thomas-Fermi screening wave vector, and $\phi = [(1 + \zeta)^{2/3} + (1 - \zeta)^{2/3}]/2$ is a spin-scaling factor, $\zeta = (n_\uparrow - n_\downarrow)/n$ is the relative spin polarization, and H is the PBE-like gradient correction with the following correlation parameter:

$$\beta = \beta_0 + \sigma t (1 - e^{-r_s^2}), \quad (5)$$

with $\beta_0 = 3\mu^{\text{MGE2}}/\pi^2$ fixed from LDA linear response, $\sigma = 0.07$ fitted to jellium surface energies, and $\alpha = 0.8$ minimizing the information entropy of an ensemble of one-electron densities [90,91].

In the construction of SRhSG4, we use the simpler expression with $\alpha = \sigma = 0$, while the coefficient β_0 will be chosen such that the entire XC functional fulfills the LDA linear response.

B. Functional construction

1. SG4 shape function and screened exchange functional

The SG4 exchange hole has been constructed in Ref. [48], using the Henderson-Janesko-Scuseria (HJS) reverse engineered model, which has the following shape

TABLE I. Parameters of the $\beta_{\text{fit}}(v)$, see Eq. (13).

a_1	a_2	a_3	a_4	a_5	β_0	β_∞
0.31949543	0.00029179	96.36612588	4.06915863	0.00000034	0.06584	0.07903

function [78]

$$\mathcal{J}^{\text{GGA}}(s, y) = \left\{ \left[\frac{9\mathcal{A}}{4y^2} + \mathcal{B} + \mathcal{C}\mathcal{F}(s)y^2 + \mathcal{E}\mathcal{G}(s)y^4 \right] e^{-\mathcal{D}y^2} - \frac{9}{4y^4} (1 - e^{-\mathcal{A}y^2}) \right\} e^{-s^2\mathcal{H}(s)y^2}, \quad (6)$$

where $\mathcal{A} = 0.757211$, $\mathcal{B} = -0.106364$, $\mathcal{C} = -0.118649$, $\mathcal{D} = 0.609650$, $\mathcal{E} = -0.0477963$ are fixed from uniform electron gas limit and the functions $\mathcal{F}(s)$ and $\mathcal{G}(s)$, and $\mathcal{H}(s)$ are fixed by the small- u behavior, normalization and energy sum rules [78]. The function $\mathcal{H}(s)$ has been computed numerically and is provided in Table II of Ref. [78].

The SR exchange enhancement factor is

$$F_x^{\omega\text{SG4,SR}}(s, \omega, k_F) = -\frac{8}{9} \int dy y \mathcal{J}^{\text{GGA}}(s, y) \text{Erfc}(\omega y/k_F) \quad (7)$$

and has an analytic form given by Eq. (43) of Ref. [78].

Finally, the screened hybrid based on the SG4 GGA functional becomes

$$E_{xc}^{\text{SRhSG4}}(\alpha, \omega) = \alpha E_x^{\text{SR-HF}}(\omega) + (1 - \alpha) E_x^{\text{SR-SG4}}(\omega) + E_x^{\text{LR-SG4}}(\omega) + E_c^{\text{SG4}}(\beta), \quad (8)$$

where $E_x^{\text{LR-SG4}}(\omega) = E_x^{\text{SG4}} - E_x^{\text{SR-SG4}}(\omega)$ and $E_x^{\text{SR-SG4}}(\omega)$ is given by

$$E_x^{\text{SR-SG4}}(\omega) = \int d\mathbf{r} n(\mathbf{r}) \epsilon_x^{\text{LDA}} F_x^{\omega\text{SG4,SR}}(s, \omega, k_F). \quad (9)$$

The coefficients

$$\alpha = 1/4, \quad \omega = 0.11 \text{ bohr}^{-1} \quad (10)$$

are fixed from the adiabatic connection method [92], and by fitting the band gap of few semiconductors [93], respectively. Same values of the parameters are used in HSE and HSEsol functionals.

2. Correlation energy functional from linear response criterion

The LDA linear response formalism applied to SR screened hybrid has been developed in Ref. [81], and the second-order correlation coefficient must be

$$\beta = 3[\mu_x^{\text{SRhSG4}}(\alpha, v)]/\pi^2, \quad (11)$$

where $v = \omega/k_F$ and μ_x^{SRhSG4} is the second-order exchange coefficient of the SRhSG4 functional [81]

$$\mu_x^{\text{SRhSG4}}(\alpha, v) = \alpha \mu_x^{\omega\text{SR-HF}}(v) - \alpha \mu_x^{\omega\text{SG4,SR}}(v) + \mu_x^{\text{SG4}}, \quad (12)$$

where $\mu_x^{\omega\text{SR-HF}}(v)$ is given by Eq. (13) of Ref. [81], $\mu_x^{\omega\text{SG4,SR}}(v)$ is the second-order coefficient of $F_x^{\omega\text{SG4,SR}}(s, \omega, k_F)$ having the expression of Eq. (10) of Ref. [81], and $\mu_x^{\text{SG4}} = \mu_x^{\text{MGE2}}$.

Finally, for the simplicity of computational implementation, we accurately fit the difficult expression of β with the

simple function

$$\beta_{\text{fit}}(v) = \frac{\beta_0 + a_1 v + a_2 v^2 + \beta_\infty a_3 v^3}{1 + a_4 v + a_5 v^2 + a_3 v^3}, \quad (13)$$

with $\beta_\infty = 3\mu_x^{\text{MGE2}}/\pi^2$, and $\beta_0 = \frac{3}{\pi^2}(\alpha \frac{7}{81} - \alpha \mu_x^{\text{MGE2}} + \mu_x^{\text{MGE2}})$, and the fitted parameters are shown in Table I.

We remark that the differences of the SG4 and SRhSG4 correlation comes from the fact that the correlation energy density of the SG4 is spin-correction factor dependent [28] and β is the functional of r_s and t [28]. However, the β of the SRhSG4 correlation is the functional of r_s only and its correlation is independent of the spin-correction factor. The use of the SG4 correlation with the SRhSG4 does not give satisfactory results for the solid-state and molecular test cases and this can be understood from the fact that the satisfaction of the local density linear response is important for the entire hybrid functional, where the inclusion of the HF exact exchange makes the exchange nonlocal. Therefore, more nonlocality information through the t in the SRhSG4 functional most probably makes the functional worse for solid-state systems. Also, the error cancellation of the exchange and correlation for the present choice of the $\beta = \beta_{\text{fit}}(v)$ is more intense.

3. Analysis of correlation potential

Recently we have shown [98] that the popular hybrid and range-separated hybrid XC functionals reproduce quite reasonable the physical features of exact correlation potential. In this paragraph, we will utilize the same methodology to investigate the correlation potential behavior provided by HSE06, HSEsol, and SRhSG4 XC functionals.

Due to explicit orbital dependence of their XC energy expressions via $E_x^{\text{SR-HF}}$ term, the corresponding correlation potential $[v_c(\mathbf{r}) = \delta E_c[\rho]/\delta \rho(\mathbf{r})]$ can be computed using OEP formalism as in Ref. [98], where the correlation energy functional by definition reads

$$E_c = E_{xc} - E_x^{\text{EXX}}, \quad (14)$$

where E_x^{EXX} being the EXX energy expressions. The functional derivatives of Eq. (14) have been computed in a post-SCF fashion for fixed reference densities obtained at exchange-only OEP (OEPx) [85,99] level. We note that this approach was already successfully utilized in many studies [100–105] to investigate the most relevant features of the XC, correlation and kinetic potentials. As in our previous studies [95,103,106–110] in order to solve OEP equation we have employed the finite-basis set procedure from Refs. [99,111]. For more technical details regarding the OEP procedure and calculations we refer the reader to Refs. [95,112].

In Fig. 1 we report the correlation potentials [corresponding to Eq. (14)] for two representative cases, namely Ar atom (left) and CO molecule (right). One can immediately note that for both systems, all functionals provide very physical

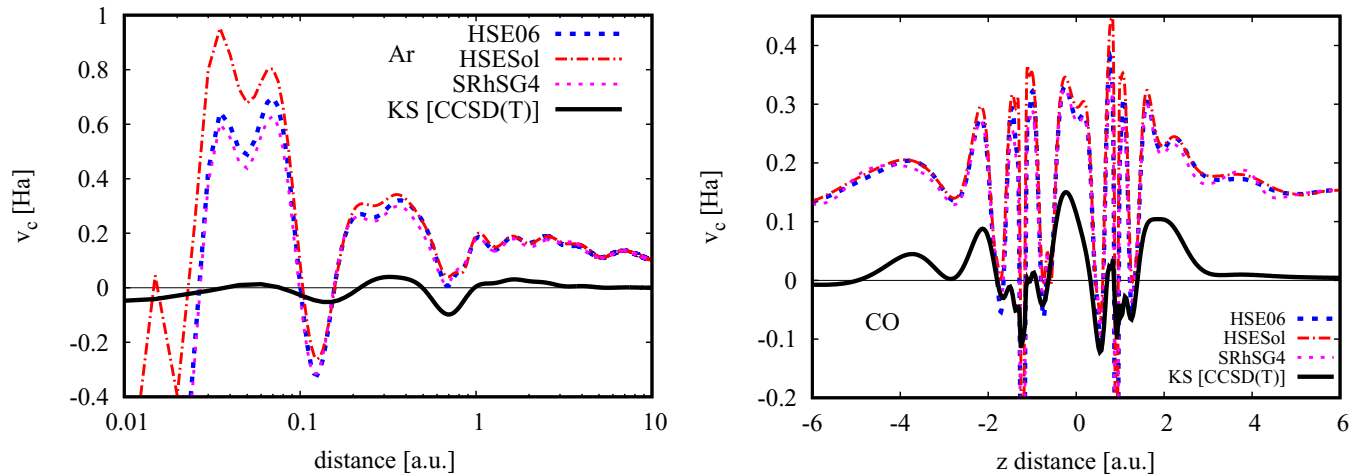


FIG. 1. The correlation potential of Ar atom (left) and CO molecule (right, along the z axis) for several XC functionals. The potential for Ar atom was generated using modified, uncontracted ROOS-ATZP [94] basis set as in Ref. [95], whereas the CO molecule were treated in uncontracted cc-pVTZ basis set of Dunning [96] at equilibrium geometry ($R = 1.128 \text{ \AA}$). The reference KS[CCSD(T)] have been obtained using method from Ref. [97] using the same basis sets.

correlation potential recovering similar quantum oscillations as the reference [coupled-cluster singles-doubles with perturbative triples [113]—CCSD(T)] curve. In the core region, all functional diverge. This feature is inherited from the GGA part of the potential depending explicitly on the Laplacian of the density ($\nabla^2 n$) which diverges in this region [114,115]. In the tail of the density, in turn, we observe that investigated potentials vanish much slower than CCSD(T) one. This is directly related to the difference in the asymptotic behavior between OEPx ($-1/r$) and hybrid potential which decay much faster, thus in the tail, the difference $v_{xc}(\mathbf{r}) - v_x^{\text{OEPx}}(\mathbf{r})$ gives the rise to significant errors in v_c which might project on the quality of ionization and excited state energies. However, we recall, that region is not relevant for most of ground state properties. While HSE06 and SRhSG4 give for both systems quite similar performance the HSEsol [80] functional exhibits slightly worse behavior being more overestimated in the core region.

4. Application to model system

As an example of a model system, we have considered the harmonium atom [116] for various values of confinement strength k . We recall, that at small values of k , the system is strongly correlated, whereas for large values of k it is tightly bounded. These two regimes are very important for many condensed matter applications. Thus harmonium atom provides an excellent tool for testing approximate density functional methods [117,118]. Alike in Ref. [105] the calculations have been performed using an even-tempered Gaussian basis set from Ref. [119] for $k \in [0.03, 1000]$. As a reference, we used full configuration interaction (FCI) results calculated in the same basis set which have been proved to be close to exact values [105].

In Fig. 2, we show the relative error (RE) on total energies calculated with respect to the FCI data for several XC hybrid functionals in the function of k . The latter energies have been obtained in post-SCF fashion on top of OEPx densities.

For comparison, we also report the MP2 [120] and *ab initio* OEP2-sc [110,121] results. We see that when $k \rightarrow \infty$ all methods start to behave similarly giving quite accurate results. In the medium- and strong-correlated limits they all start differ significantly. The MP2 and OEP2-sc for $k < 1$ produce quite large errors. The XC DFAs, however, perform quite well for $k \geq 1$. This is due to the shrinking HOMO-LUMO gap (present in the denominator of energy expression MP2 and OEP2-sc correlation) with a decrease of confinement strength. The best results are obtained for the SRhSG4 functional which outperforms all the other approximations giving an overall mean absolute relative error (MARE) of 0.19%. This is probably due to the balanced error cancellation effect between the exchange and correlation part of the XC functional. The HSE06 and SG4 functionals, in turn, give here 0.22% and 0.29%, respectively. The biggest error between DFAs is given by HSEsol functional which yields overall MARE of 1.03%.

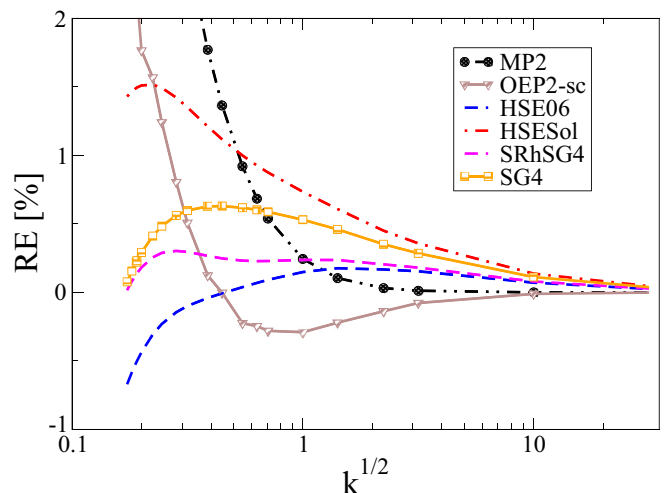


FIG. 2. Relative error on total energies of harmonium atoms for various values of confinement strength k .

TABLE II. Mean errors (MEs) and mean absolute errors (MAEs) for equilibrium lattice constants, bulk moduli, and cohesive energies of a set of 20 bulk materials. The best (worst) results of each line are in boldface (underlined). The reference values of the present calculations are taken from Ref. [127].

Test set	Errors	SG4	SRhSG4	HSEsol	HSE06
Lattice constants (Å)					
LC20	ME (Å)	0.004	-0.012	-0.014	0.029
	MAE (Å)	0.029	0.018	0.018	0.032
Bulk moduli (GPa)					
BM20	ME (GPa)	0.39	2.81	3.42	-3.64
	MAE (GPa)	6.88	5.66	5.98	6.26
Cohesive energies (eV/atom)					
COH20	ME (eV/atom)	0.161	0.017	-0.082	-0.259
	MAE (eV/atom)	0.254	0.177	0.177	0.269

III. APPLICATION TO SOLID-STATE PROPERTIES

A. Computational details

To assess the solid-state performance of the SRhSG4 we implement the functional form in the plane wave pseudopotential code *Vienna Ab initio Simulation Package* (VASP) [122–125]. The VASP recommended pseudopotential with $12 \times 12 \times 12$ Γ -centered \mathbf{k} points are used for all bulk calculations. For the cohesive energies, the atoms are placed in an orthorhombic box of size $16 \times 17 \times 18 \text{ \AA}^3$. For polar molecules, the dipole correction is also applied to avoid interactions between dipoles.

The lattice constants are calculated by relaxing the unit cell volume using the Gaussian smearing. For ionic relaxation, we used the conjugate gradient algorithm.

The bulk moduli are obtained from fitting the energy per unit cell versus volume curve with the third-order Birch-Murnaghan isothermal equation of state. The volume of the unit cell is varied in the range $V_0 \pm 5\%$, where V_0 is the equilibrium volume.

The cohesive energies of solids are equivalent to the atomization energies of molecules and it is defined as the energy required per atom to atomize the crystal as

$$E_{\text{coh}} = E_{\text{atom}} - \frac{E_{\text{bulk}}}{N}, \quad (15)$$

where E_{atom} is the atomic energy and E_{bulk} is the bulk energy of the unit cell having N atoms.

For completeness, the functional is also benchmarked for several atomic and molecular tests with the NWChem program package [126] using the Gaussian basis set.

B. Lattice constants, bulk moduli, and cohesive energies

Accurate prediction of lattice constants of solids is quite important. Other equilibrium properties depend on the accuracy of the lattice constants. For example, the ferroelectric properties are strongly influenced by an accurate prediction of the lattice constants. To assess the functional performance for the solids, we consider the set of 20 strongly bound solids compiled in Ref. [127], often used to assess the performance of newly developed XC density functionals [9]. This test set comprises equilibrium lattice constants (LC20), bulk moduli

(BM20), and cohesive energies (COH20) of 20 solids. This test set consists of six simple metals (Li, Na, Ca, Sr, Ba, and Al), four transition metals (Cu, Rh, Pd, and Ag), five semiconductors (C, Si, Ge, SiC, and GaAs), and five ionic solids (LiF, LiCl, NaF, NaCl, and MgO).

In Table II, we report the mean error (ME) and mean absolute error (MAE) for LC20, BM20, and COH20, as obtained from different screened hybrid functionals. For comparison, the SG4 error is also shown. To calculate the error of LC20 test, we consider the zero-point an-harmonic expansion (ZPAE) corrected experimental lattice constants from Ref. [127]. Our results show that SRhSG4 is remarkably accurate for the lattice constants of solids, further improving the SG4 results by reducing its MAE with $\sim 10 \text{ m\AA}$. We mention that SG4 is one of the state-of-art semilocal GGA functionals for lattice constants of strongly bound bulk solids [7,28]. The HSEsol functional is also as accurate as SRhSG4, while the HSE06 functional is deviating more. Nevertheless, all the considered SR hybrid functionals (HSE, HSEsol, and SRhSG4) are improving considerably over their GGA functional (PBE, PBEsol, and SG4). We recall that for the LC20 test, PBE gives MAE = 0.060 \AA , and PBEsol gives MAE = 0.035 \AA .

To depict the detailed performance of the SRhSG4, we plot in Fig. 3 the relative error (RE in %) of each solid for LC20 (left panel), BM20 (middle panel), and COH20 (right panel), as obtained from the considered functionals. As shown in the left panel of Fig. 3, SRhSG4 improves over SG4 for simple metals (Ca, Sr, Ba), semiconductors (Ge, SiC, GaAs), and ionic crystals (LiF, NaF, NaCl, MgO). This is probably due to the partial reduction of the SG4 exchange by the short-range HF and the satisfaction of the LDA linear response. We also remark that SRhSG4 and HSEsol give almost the same results, with exception of transition metals, where SRhSG4 is slightly better for Cu, Rh, and Pd (indicating the accuracy for larger values of Z), but worse for Ag. Finally, we observe that HSE06 overestimates the lattice constants which is well known as it follows from the overestimation of the PBE functional.

The bulk modulus is defined as the volume variation with the external pressure [128]. This is an important quantity related to the structural phase stability of different phases of solids and to the hardness [129]. In Table II, the error statistics of considered functionals are summarized. SRhSG4

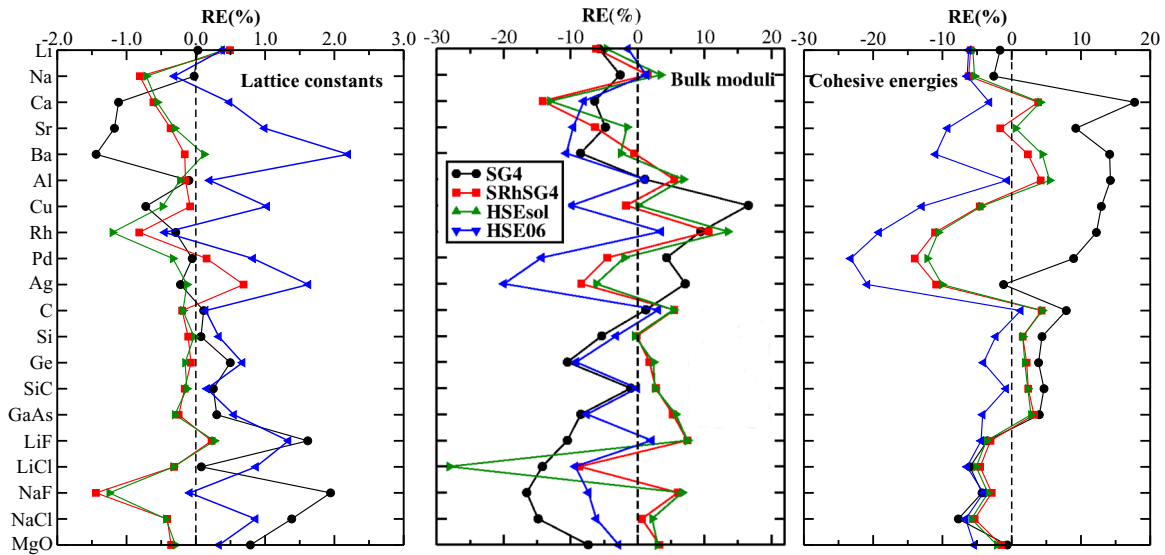


FIG. 3. RE (in %) of the lattice constants (left panel), bulk moduli (middle panel), and cohesive energies (right panel) as obtained from different functionals for the set of 20 bulk solids.

is the most accurate functional within the considered screened hybrids with MAE = 5.66 GPa, better than HSEsol (MAE = 5.98 GPa), HSE06 (MAE = 6.26 GPa), and SG4 (MAE = 6.88 GPa). Physically, the short-range HF which is mixed with the SG4 functional improves the energetic as well as lattice constants of solids implying the improvement of SRhSG4 for the bulk moduli. The errors of the SG4 and HSE06 stream from the energetic and lattice constants of bulk solids, respectively. For a better comparison, in the middle panel of Fig. 3, we show the RE of the considered functionals. We observe that SRhSG4 performs slightly better than HSEsol for simple metals and ionic crystals, while for the other solids both perform almost similarly.

The cohesive energy is also an important energetic property for solids, measuring the corresponding binding energies between the finite and infinite bulk solid unit cells, respectively. A functional which is good for solid-state lattice constants can perform modestly for cohesive energies. For example, PBEsol is much better than PBE for determining the lattices but not as good as PBE for cohesive energies. Recently, it was also shown that the SCAN meta-GGA functional is not so good as PBE for the cohesive energies of the alkali metals [130,131], despite its better performance for the solid-state lattice constants. In fact, a functional accurate for cohesive energies of bulk solids must give a good balance between the descriptions of slowly varying valence densities of bulk solids, and moderately and rapidly varying valence densities of atoms. In this respect, we observe that both SRhSG4 and HSEsol perform in a better way for the cohesive energies, beating the SG4 and HSE06. Both functionals perform better than their semilocal form (i.e., SG4 and PBEsol) [28], in contrast to the HSE06, which worsens the performance of the PBE. In the right panel of Fig. 3 we plot the RE of the cohesive energies of all solids. In this case, also, slight different behavior of SRhSG4 and HSEsol is observed for simple and transition metals, indicating the importance of the local density linear response in case SRhSG4.

To analyze the errors obtained from all considered functionals, we calculate the Wilcoxon signed-rank test for the pair of methods. This test can indicate the statistical difference between the pair of functionals.

In Table S1 [132], we report the Wilcoxon signed-rank test values (W) along with the associated p values. As the size of the data used in this case is 20, the Wilcoxon W statistic tends to form a normal distribution. The null hypothesis is used for each error pairs [133]. Here, the pairs of methods with $W < W_{\text{crit}}$ and $p > 0.05$ lack statistically significant difference in their outcomes. Analyzing the p values, we do not observe significant statistical differences in the absolute error distributions of SRhSG4 and HSEsol for lattice constants, bulk moduli, and cohesive energies.

Overall, the satisfaction of the local density linear response is an important constraint for the hybrid functional construction, especially for the structural properties of the solids. Further, the satisfaction of the semiclassical atom theory makes the constructed SRhSG4 quite a good performer. Overall, the constructed functional is competitive with the HSE06 and HSEsol functionals.

C. Magnetic properties of Fe, Co, and Ni

Density functional theory is a powerful tool in the field of the magnetization. Semilocal functional, especially the prototype PBE functional, often performs remarkably for the different magnetic properties. Other techniques like PBE + U, hybrid density functionals, and many-body perturbation theory (RPA, MBPT, and GW) are also applied to metallic $3d$ elements. When a new density functional is proposed it is always a common practice to determine ground-state properties of the Fe. The stable phases of Fe that are found experimentally are bcc, fcc, and hcp. However, the magnetic bcc phase is the most stable phase compared to the nonmagnetic hcp and fcc counterparts. Regarding the common GGA functionals performance, the PBE provides the correct description of the

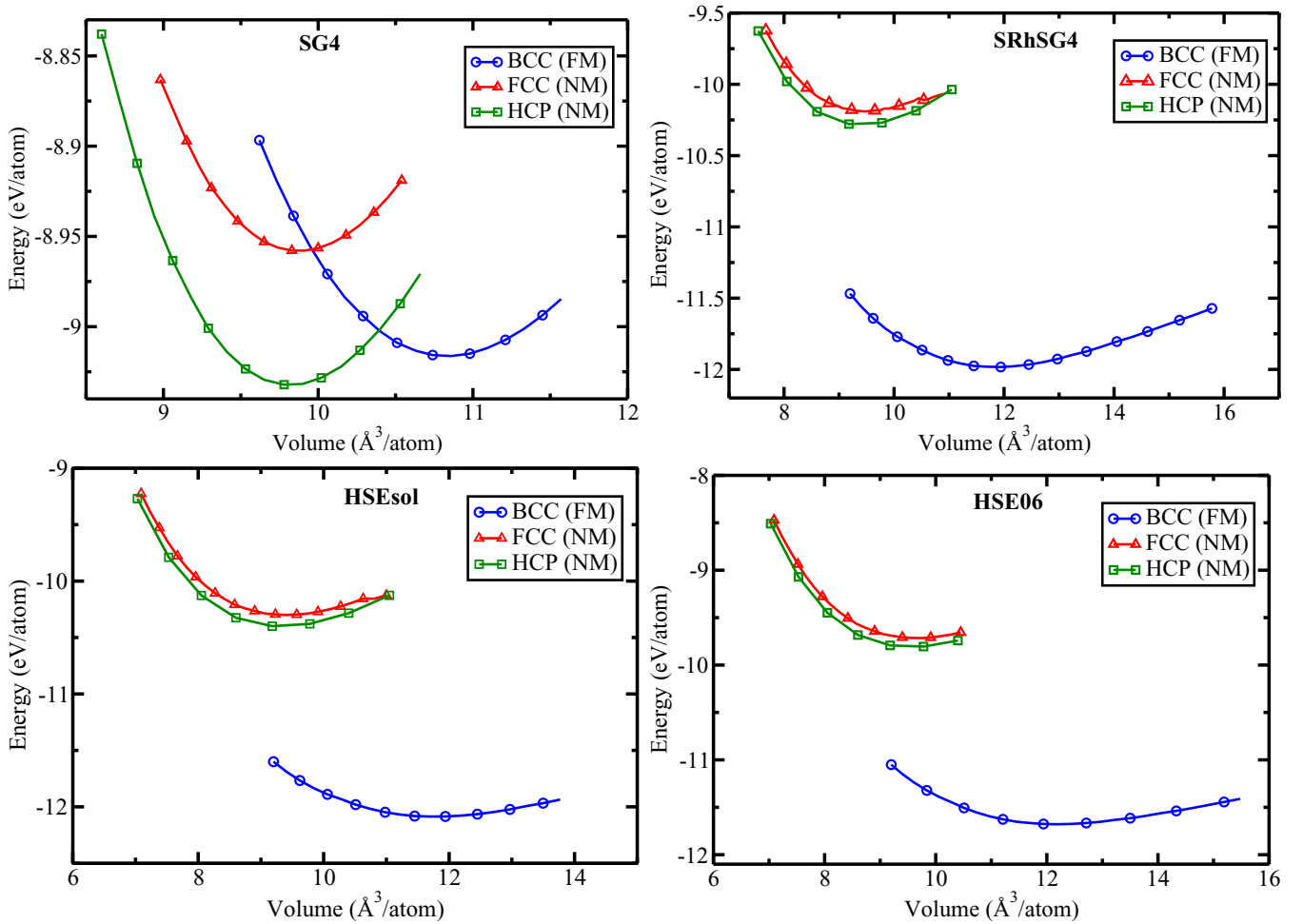


FIG. 4. Energy versus volume curves of different phases of Fe as obtained from several methods.

Fe phases [130,134], while PBEsol predicts the nonmagnetic fcc to be the most stable phase [135]. Note that meta-GGA, RPA and hybrid density functionals also correctly predict the magnetic bcc as the most stable phase [130,134,136–139]. The energy differences of bcc, hcp, and fcc phases of Fe as obtained from RPA are $E_{\text{bcc-hcp}}^{\text{RPA}} = -0.13$ eV/atom and $E_{\text{bcc-fcc}}^{\text{RPA}} = -0.18$ eV/atom respectively [138]. While for PBE those are $E_{\text{bcc-hcp}}^{\text{PBE}} = -0.083$ eV/atom and $E_{\text{bcc-fcc}}^{\text{PBE}} = -0.153$ eV/atom, respectively [138].

Here, we apply the screened hybrid density functionals to perform the total energy calculations for the ground-state properties of bcc, hcp, and fcc phases of Fe. The variation of the energy versus volume curve of all the phases are shown in Fig. 4. We found that the SG4 semilocal functional predicts the nonmagnetic hcp as the most stable state similar to the PBEsol [135]. However, the screened hybrid functional of the SG4, i.e., SRhSG4 correctly gives the magnetic bcc Fe to be the ground state followed by the nonmagnetic hcp and fcc structure. The HSEsol also shows the same trend, correcting the behavior of the PBEsol. However, both the PBE and HSE correctly describe the ordering of phases.

We also determine the energy differences of the magnetic bcc and nonmagnetic hcp and fcc phases for the hybrids.

We find $E_{\text{bcc-fcc}}^{\text{SRhSG4}} = -1.79$ eV/atom and $E_{\text{bcc-hcp}}^{\text{SRhSG4}} = -1.70$ eV/atom for SRhSG4, performing similar to the HSEsol, for which we obtain the energy differences as $E_{\text{bcc-fcc}}^{\text{HSEsol}} = -1.78$ eV/atom and $E_{\text{bcc-hcp}}^{\text{HSEsol}} = -1.68$ eV/atom. For HSE06 these energy differences are $E_{\text{bcc-fcc}}^{\text{HSE06}} = -1.95$ eV/atom and $E_{\text{bcc-hcp}}^{\text{HSE06}} = -1.86$ eV/atom, respectively. Note that these values are much larger than the PBE and RPA ones [138]. This is probably due to the inclusion of the HF exchange, which makes the magnetic Fe bcc phase more stable than others.

In supporting information [132], we have shown the energy versus volume plots of the different phases of Co and Ni [142,143]. For Co phases, all functionals give the hcp Co as the most stable one rather than its fcc and bcc phases. For Ni phases also all functionals predict the fcc as the most stable one. Contrary to the screened hybrids, in this case, the SG4 predicts hcp more stable than bcc.

Finally, we turn to the magnetic moments and relaxed volumes of the magnetic Fe, Co, and Ni structures as obtained from different screened hybrids and SG4 semilocal functionals, and those are reported in Table III. It is well known that the hybrid functionals generally lead to higher magnetic moments in metals [81,139,144], while the volume is comparable to the experimental values. The magnetic moments obtained

TABLE III. Equilibrium volumes (in \AA^3) and magnetic moments (M_s/atom in μB) of Fe (bcc), Co (fcc), and Ni (fcc), computed using different SR hybrid functionals. All calculations are performed using the $11 \times 11 \times 11$ Γ centered \mathbf{k} points with default PAW pseudopotentials and energy cutoffs.

Solids	Magnetic Ordering		SG4	SRhSG4	HSEsol	HSE06	Expt. ^a
Fe (bcc)	FM	V_0	10.74	11.80	11.75	12.03	11.64
		M_s	2.08	2.97	2.97	2.99	1.98, 2.08, 2.13
Co (hcp)	FM	V_0	10.35	10.33	10.26	10.99	10.96
		M_s	1.66	1.91	1.91	2.06	1.52, 1.55, 1.58
Ni (fcc)	FM	V_0	10.40	10.42	10.34	10.66	10.81
		M_s	0.66	0.87	0.87	0.91	0.52, 0.55, 0.57

^aSee Ref. [134] and all references therein and Table I of Ref. [134].

from the SG4 functional are better than the ones predicted by SG4 hybrids. This indicates that the inclusion of the HF exchange leads to a possible overestimation of the spin up density of states, and/or an underestimation of the spin-down states [139].

D. Structural phase transitions of Si and Zr

Next, we investigate the structural phase transition parameters of the crystalline solids Si and Zr under pressure. Our investigated properties involve the energy difference, volume difference, and transition pressure of the two polymorphs of a solid. Note that the accurate prediction of transition pressure needs good performance for the geometries and energies of the two solid polymorphs simultaneously, and most of the density functionals fail to do that. Recent studies showed that the meta-GGA functionals obeying the strongly tightened bound such as MGGA-MS, MVS, and SCAN are very successful in predicting the phase transition parameters [140,145,146]. Regarding the Si, the two most stable phases are diamond-Si (D-Si) [high-pressure phase (HP)] and β -tin Si (β -tin Si) [low-pressure phase (LP)]. For Zr, the two most stable phases are ω -Zr [high-pressure phase (HP)] and β -Zr [low-pressure phase (LP)].

In Table IV, we summarize the optimized structural properties and phase transition parameters of the D-Si and β -tin

Si phases as obtained from different screened hybrid density functionals. The equilibrium lattice parameters and volume of the D-Si typically show the same trend as we obtained in our previous analysis. The HSE06 slightly overestimates the equilibrium geometries, whereas the SRhSG4 and HSEsol are in the good agreement with the experimental and quantum Monte Carlo (QMC) results [141]. For the LP β -tin Si phase, all the screened functionals are in good agreement with the QMC data [141], but SRhSG4 and HSEsol are slightly better than HSE06.

Regarding the semilocal SG4 functional, it does not perform as accurately as the three collective screened hybrids. It underestimates the energy differences severely, like other GGA functionals [140]. However, all three hybrids agree quite well for the transition pressures (P_t) of the two Si phases, being closer to the QMC data [141].

Now we turn into structural and phase transition parameters of ω -Zr and β -Zr. The results are summarized in Table V. As can be seen from Table V, both SRhSG4 and HSEsol quite accurately predict the lattice constant of the LP phase of Zr, i.e., ω -Zr. The c_0/a_0 as obtained from both the functionals are close to the experimental one. However, HSE06 underestimates slightly the a_0 and overestimates c_0/a_0 . In comparison, the SG4 underestimates the a_0 but predicts c_0/a_0 ratio quite well. However, for β -Zr the trends are somehow different. In this case, HSE06 performs better than SRhSG4 and HSEsol

TABLE IV. Structural and phase transition parameters of the D-Si and β -tin Si, as obtained from different functionals.

System	Properties	SG4	SRhSG4	HSEsol	HSE06 ^a	QMC ^b	Ref. ^a
D-Si (LP)	a_0	5.378	5.409	5.414	5.433		5.415, 5.4288
	V_0 ($\text{\AA}^3/\text{atom}$)	19.450	19.785	19.862	20.05	19.98	19.914, 20.0
	B	95.48	100.7	100.4	101.5, 99.1	98	100.8, 99.2, 97.88
	B'	4.16	4.09	4.08	4.06, 4.00	4.6	4.11, 4.24
	a_0	4.7230	4.7966	4.7903	4.7602		
β -tin Si (HP)	c_0/a_0	0.553	0.540	0.539	0.5491, 0.565	0.550	
	V_0 ($\text{\AA}^3/\text{atom}$)	14.585	14.9025	14.825	14.81, 15.10	15.2	
	B	124.01	122.9	125.6	119.0, 117.0	107	
	B'	4.50	4.45	4.42	4.32, 4.35	4.6	
	Phase transition parameters						
	ΔE_0 (eV/atom)	0.091	0.378	0.336	0.398, 0.390, 0.447	0.424	
	ΔV_0 ($\text{\AA}^3/\text{atom}$)	4.87	4.88	5.037	5.35	4.368	
	P_t (GPa)	3.05	13.54	11.55	13.3, 12.4	14.0 \pm 1.0	10–14, 11–15

^aRef. [140] and all references therein and Table I of Ref. [140].

^bRef. [141].

TABLE V. Structural and phase transition parameters of the ω -Zr and β -Zr, as obtained from different functionals.

System	Properties	SG4	SRhSG4	HSEsol	HSE06 ^a	Ref. ^a
ω -Zr (hcp) (LP)	a_0	4.970	5.032	5.031	5.024	5.039, 5.050
	c_0/a_0	0.6251	0.6245	0.6245	0.6270	0.6251, 0.6237
	V_0 ($\text{\AA}^3/\text{atom}$)	22.15	22.11	21.99	22.96	23.09
	B	99.3	103.8	103.8	91.05	104, 90, 109
	B'	3.54	3.52	3.68	3.34	2.05, 4.0
β -Zr (bcc) (HP)	a_0	3.513	3.553	3.517	3.5774	3.574, 3.570
	V_0 ($\text{\AA}^3/\text{atom}$)	21.70	21.87	21.76	22.89	22.82
	B	91.77	79.90	82.86	78.59	
	B'	2.99	8.30	8.17	3.52	
	Phase transition parameters					
	ΔE_0 (eV/atom)	0.088	0.216	0.214	0.200	
	ΔV_0 ($\text{\AA}^3/\text{atom}$)	0.458	0.235	0.235	0.065	0.270
	P_t (GPa)	23.61	—	—	—	30 ± 2

^aRef. [140] and all references therein and Table III of Ref. [140].

for a_0 and V_0 . This is probably related to the performance of the semilocal functionals used to construct the screened hybrids. Thus, PBE performs better than PBEsol [140] and SG4 GGA.

Considering the phase transition parameters of Zr phases, the volume difference, ΔV_0 calculated by SG4 is almost twice bigger than the experimental one. While HSE06 value is almost one order of magnitude smaller. This is because the volumes of ω -Zr and β -Zr as predicted from HSE06 are very close to each other and hence the underestimation. In this case, both SRhSG4 and HSEsol perform similarly, giving the ΔV_0 in good agreement with the experimental one. Note that for transition pressure, all the screened hybrid functionals are unsuccessful.

Overall, the structural phase transition parameters are predicted in an improved way with SRhSG4 and HSEsol functionals. Except for the phase transition pressure of Zr, SRhSG4, and HSEsol perform better than HSE06. The drawback of all the screened functionals for metal Zr transition pressure can be explained from its wrong screening for metals [147–149] and can be improved by using the middle range-separated hybrid and/or dielectric dependent hybrid based on SRhSG4 and HSEsol functionals.

E. Ferroelectric properties of BaTiO₃ and PbTiO₃

ABO₃ type ferroelectric materials are quite important in various technological and industrial applications. The crystal type of ABO₃ ferroelectric is known as perovskite, where the polar distortion is originated from the off-centering displacement of B ion. In this category, the prototype ferroelectric materials are BaTiO₃ and PbTiO₃, which are considered as particular examples in this study to assess the performance of the constructed screened hybrid density functional. Both BaTiO₃ and PbTiO₃ have been extensively studied previously and experimental reference values are available to directly compare the functional performance. Among the most recent investigations, we find that Zhang *et al.* [150] studied prototype ferroelectric materials using the LDA, GGA, meta-GGA, and screened hybrid density functionals. Several other studies based on the global and screened hybrid density functionals

are also found [155,161–164]. Note also that studies involving the model Hamiltonian technique are also available [164,165].

Regarding the interactive nature of the ATiO₃ (where A = Ba and Pb), A-O bond is essentially ionic, while in Ti-O bond both ionic and covalent interaction is important. Due to this diverse bonding nature, ferroelectric materials are typically challenging for semilocal density functional XC approximations. In Table VI, we calculate the various structural and ferroelectric properties of the ATiO₃ (A = Ba and Pb). In general, for BaTiO₃ the hybrid density functionals perform better than their corresponding semilocal form, which is reflected in the performance of the SRhSG4, where the tetragonality of the SG4 is reduced by SRhSG4 functional, indicating the ionic and covalent bonds are more elegantly treated by SRhSG4 than SG4. Similar logic is also applied for HSEsol. Both the SRhSG4 and HSEsol perform in the same degree of accuracy for BaTiO₃, slightly better than HSE06 for tetragonality and spontaneous polarization, but not as good as HSE06 for the energy difference of the paraelectric (PF) and ferroelectric (FE) phases (ΔE). In fact, all tested XC functionals are typically giving the ΔE within ~ 11 meV/atom [150].

Next, we calculate the structural and ferroelectric properties of another prototype ferroelectric of ATiO₃, i.e., PbTiO₃. The lattice constants as predicted from the SRhSG4 and HSEsol are slightly smaller than the HSE06. Typically, SRhSG4 improves over SG4 for all the structural and ferroelectric properties. Slightly smaller off-center displacement of the Ti from its position indicating the smaller polarization for SRhSG4 than SG4 and HSE06. The polarization of the PbTiO₃ as predicted from SRhSG4 is about $111.8 \mu\text{C}/\text{cm}^2$ which is within the range of the experimental values. Also, the SRhSG4 performs significantly better than SG4 for the structural phase transition energies (ΔE) from the cubic paraelectric (PF) to noncubic ferroelectric (FE) phases.

Overall, the SRhSG4 functional performs as good as HSE06 and HSEsol for the structural and ferroelectric properties of the prototype ABO₃ type ferroelectric. Different bonding nature is well captured by the SRhSG4, indicating its improvement over SG4 for the tetragonality problem. This is due to the HF mixing, which also reduces the delocalization error of the semilocal functional and improving the band gap.

TABLE VI. Comparison of calculated and experimental values of the structural, ferroelectric, and electronic properties of the BaTiO₃ and PbTiO₃ orthorhombic crystals as obtained from different XC functionals. ΔE corresponds to the energy difference of the paraelectric (PF) and ferroelectric (FE) phases. The HSE06 values are taken from Ref. [150].

Methods	Lattice (a_0)		Volume (V_0) \AA^3	Displacement (Δr_i) (in units of the lattice constant c)	Polarization (P_x) ($\mu\text{C}/\text{cm}^2$)	$E_{PF}-E_{PE}$ (ΔE) (meV/atom)	Band gap (E_g) eV
	\AA	Tetragonality (c/a)					
BaTiO ₃							
SG4	3.944	1.054	64.7	0.013	41.9	2.12	1.71
SRhSG4	3.942	1.031	63.2	0.017	35.3	5.5	3.26
HSEsol	3.940	1.027	62.8	0.018	33.7	5.6	3.25
HSE06	3.959	1.039	64.5	0.019	40.7	10.8	3.27
Exp	3.986 ^a	1.010 ^a	64.0 ^a	0.015 ^a	26 ^b	34 ^c	3.27 ^d , 3.38 ^d
PbTiO ₃							
SG4	3.804	1.227	67.5	0.056	126.4	7.1	1.75
SRhSG4	3.792	1.180	64.4	0.043	111.8	19.8	2.97
HSEsol	3.793	1.183	64.5	0.049	114.2	20.6	2.93
HSE06	3.832	1.158	65.2	0.047	114.4	38.8	3.00
Exp	3.880 ^e	1.071 ^e	62.6 ^e	0.040 ^f	57 ^g , 75 ^h , 90–100 ⁱ	67 ^j	3.6 ^k

^aRoom temperature measurements [151].

^bLow temperature measurements [152].

^cData at 393K [153].

^dRef. [154].

^ezero temperature value [155].

^fRoom temperature measurements [156].

^gRef. [157].

^hRef. [158].

ⁱRef. [159].

^jData at 760K [153].

^kRef. [160].

Finally, it is important to note that some lattice constants and polarization are measured at very high temperatures, such that a direct comparison with 0 K calculations is not always meaningful. For example, the BaTiO₃ lattice constants and off-center displacement are measured at room temperature. The polarization is measured at low temperature and the paraelectric to ferroelectric phase transition is calculated at 393K. Similarly, for PbTiO₃, the displacement and the ferroelectric phase transition energy are calculated at room temperature and 760 K, respectively.

F. Band gaps and optical properties

1. Band gaps

It is well known that the semilocal functionals suffer from the delocalization error, whereas the HF suffers from localization error [34,167–172]. The screened hybrids which include part of semilocal and SR HF are capable of predict the narrow and medium-range band gaps quite accurately. In Table VII, we report the selected band gap of ten semiconductors taken from the SBG31 [166] test set. These ten semiconductors consist of only narrow and medium-range band gap solids (for example C). The SRhSG4 and HSEsol slightly lower the band gap of solids, hence perform slightly better than HSE06 for narrow band gap materials. As all the functionals include 25% HF exchange, the small decrease of the band gap energies, shown by SRhSG4 and HSEsol, comes from their semilocal version. The exchange energy density of SG4 and PBEsol are flatter than the PBE one in the region $0 < s < 2$, slightly lowering the orbital energies which in turn slightly

lower the generalized KS gap of the SRhSG4 and HSEsol functionals with respect to the HSE06 band gap results. We also report the MARE of the full SBG31 [166] test set in the last column of Table VII. Overall, all functionals perform similarly. However, HSE06 is slightly better than SRhSG4 and HSEsol for medium and wide band gap solids. Note that the

TABLE VII. The band gaps (in eV) of 10 selected semiconductors from the SBG31 [166] test set using different levels of approximations. For comparison, the MAREs (in %) of the band gap energies of the full SBG31 [166] test set are also provided on the last row. Being a semilocal functional, we do not consider here the SG4 functional.

Solids	SRhSG4	HSEsol	HSE06	Expt.
InSb	0.40	0.43	0.53	0.24
InAs	0.37	0.42	0.53	0.42
InN (Wurzite)	0.78	0.79	0.71	0.72
Ge	0.72	0.75	0.82	0.74
GaSb	0.78	0.83	0.91	0.82
Si	1.11	1.09	1.17	1.17
InP	1.37	1.4	1.52	1.42
GaAs	1.28	1.33	1.44	1.52
AlSb	1.72	1.72	1.8	1.69
GaN (Wurzite)	3.10	3.11	3.03	3.28
GaN	3.24	3.15	3.21	3.50
C	5.29	5.21	5.29	5.50
MARE of full SBG31 test set	14.31	14.44	14.73	

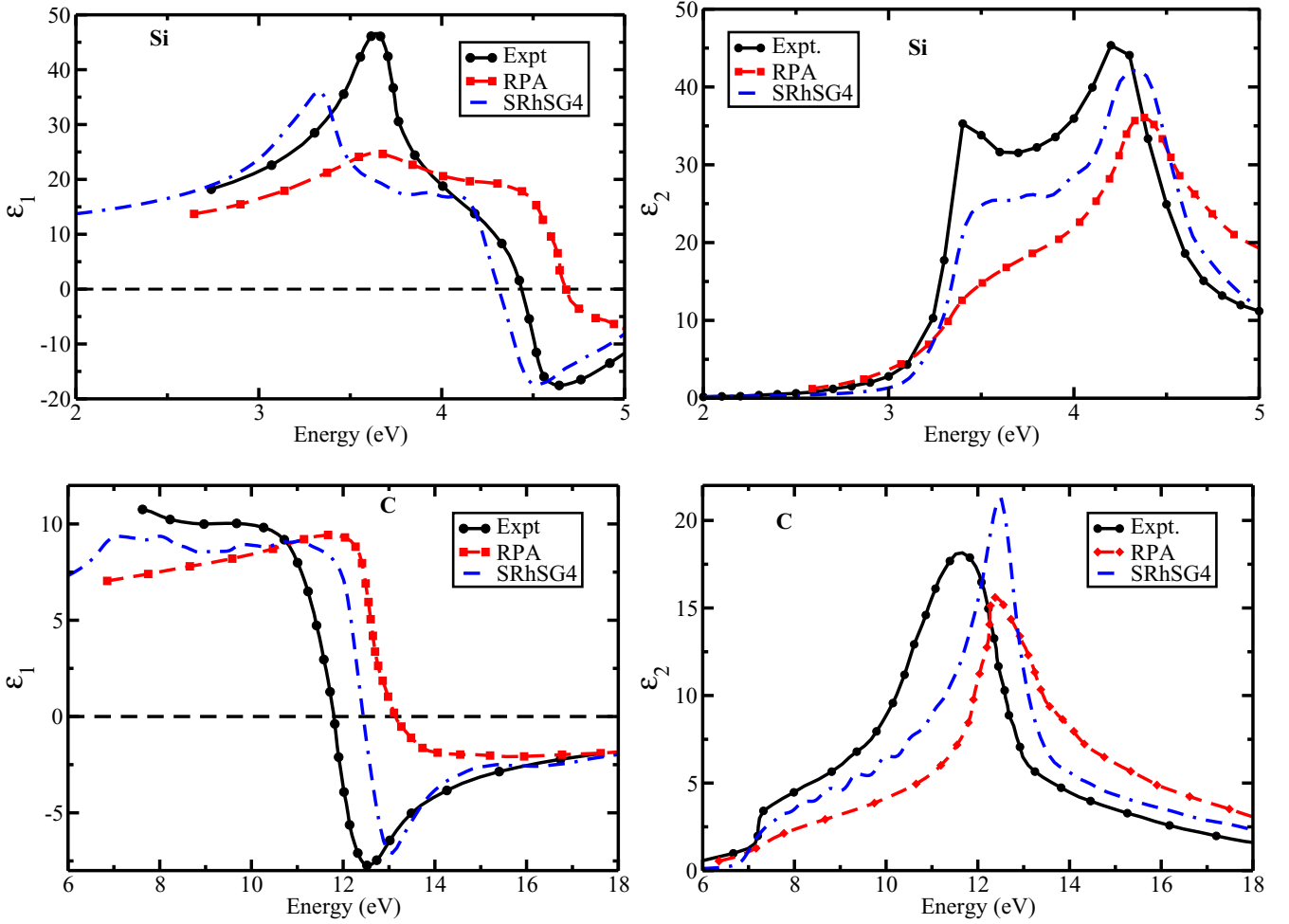


FIG. 5. $\epsilon_1(\omega)$ and $\epsilon_2(\omega)$ versus ω , for Si (upper panels) and C (lower panels), as obtained from SRhSG4 density functional. For comparison the RPA results are also shown.

screened functionals proposed based on the meta-GGA form are slightly better than HSE06 because the nonlocality information is already more enhanced in the semilocal form of the meta-GGA than GGA as shown in Refs. [47,173,174]. Overall, analyzing the Wilcoxon signed-rank test (Table S2 [132]) we observe no significant differences in the band gap performance of SRhSG4 and HSEsol functionals.

2. Optical absorption spectra from SRhSG4 functional

The screened hybrids include nonlocal orbital-dependent exchange term which is the key to the improvement of its performance for the dielectric properties of the bulk solids [39,175–178]. Typically, the optical absorption spectra as obtained from the time-dependent DFT within the RPA and adiabatic LDA (ALDA) do not include the electron-hole excitation effects. However, specially designed semilocal XC kernels are quite successful [40,179–182] for the absorption spectra of semiconductors and insulators, providing a realistic description of excitons and excitonic effects. The special advantage of the screened hybrid is that it improves the band gap of solids, captures the screening of the system, and the required excitonic effects, i.e., $\sim \frac{1}{q^2}$ in the long-wavelength limit ($q \rightarrow 0$) is well respected by HF kernel. Therefore,

the optical absorption spectra as obtained from the screened hybrids are improved and significantly better than LDA and RPA [39,175].

To assess the performance of the SRhSG4 functional we calculate the real $[\epsilon_1(\omega)]$ and imaginary $[\epsilon_2(\omega)]$ parts of the macroscopic dielectric function ϵ^M in the optical limit of small wave vectors

$$\begin{aligned}\epsilon_1(\omega) &= \Re\{\lim_{q \rightarrow 0} \epsilon^M(\mathbf{q}, \omega)\}, \\ \epsilon_2(\omega) &= \Im\{\lim_{q \rightarrow 0} \epsilon^M(\mathbf{q}, \omega)\}.\end{aligned}\quad (16)$$

The optical absorption spectrum is given by $\epsilon_2(\omega)$, while other optical properties imply both $\epsilon_1(\omega)$ and $\epsilon_2(\omega)$. For example the long-wavelength limit of the electron-energy-loss function is $\epsilon_2(\omega)/[\epsilon_1(\omega)^2 + \epsilon_2(\omega)^2]$. We consider Si and C bulk semiconductors, which are important test examples for optical properties. All calculations are performed in the VASP code using the method suggested in Ref. [39]. We use $32 \times 32 \times 32$ \mathbf{k} points with eight empty orbitals. Being very expensive, the SRhSG4 calculations are performed in many shifted $8 \times 8 \times 8$ grids [39]. The resultant $\epsilon_1(\omega)$ and $\epsilon_2(\omega)$ are shown in Fig 5. For comparison, the RPA results are also reported, being taken from Ref. [40].

The optical absorption spectrum of Si, computed with SRhSG4, is quite realistic, showing two peaks at the right positions. Nevertheless, the first peak at ~ 3.5 eV, which is associated with an oscillator strength, is underestimated. The same feature is observed for the first peak of $\epsilon_1(\omega)$, which is also slightly red shifted. However, the second, negative peak of $\epsilon_1(\omega)$ is accurately described. Overall, the performance of SRhSG4 for the optical properties of Si semiconductor is remarkable, being comparable with the results of specialized XC kernels [40]. In Ref. [39] it was suggested that different range of the screening parameter may improve the spectra which can be tested for this case also.

Next considering the optical spectra of the medium ranged semiconductor C, both the SRhSG4 and RPA spectra are rather inaccurate. The SRhSG4 and RPA peaks are both blueshifted with about 1 eV. However, the SRhSG4 gives an important improvement over RPA in the whole energy range, from 6 to 18 eV. The SRhSG4 improvement over RPA is even more evident for $\epsilon_1(\omega)$, where the SRhSG4 curve is closer to the experimental one, being able to describe the negative peak at around 12 eV, even if it is blueshifted with about 0.5 eV. We recall that the optical properties can be further improved by making ω or α system-dependent via the inclusion of density and gradient of density [183,184], and/or dielectric dependence [185–190].

G. Performance for small molecules

Last, we assess the functionals for some well-known molecular test cases. Ideally, a functional accurate for solid-state test cases should also provide reasonable good energy differences for molecular systems. In general, for molecules, the long-range corrected or global hybrids perform well [55]. However, at the GGA level, simultaneous good performance for both chemical and solid-state worlds are quite difficult. Though global hybrid PBE0 [191] works reasonably well for chemical applications, it is not so popular for solid-state physics.

In Table VIII, we summarize MAE of several test sets as obtained from different screened hybrids considered in this paper. We consider the Minnesota 2.0 test set [166] to assess the functionals performance. For atomization energies (AE6 and G2/148) HSEsol is the worse performing functional. It is reasonable because in the semilocal level PBEsol is already bad for molecular atomization energies. This is due to the restoring of the density-gradient expansion (GE2) for exchange. However, SG4 satisfies the semiclassical atom theory and MGE4, which makes it reasonably well performer both for the general-purpose molecular test cases as well as solids, being better than PBEsol [28]. Note that SG4 is as accurate as PBE at the semilocal level because of the satisfaction of MGE4. Therefore, the improved atomization energies for SRhSG4 are not surprising and quite reasonable because of the inclusion of the HF exchange. For atomization energies, SRhSG4 is as accurate as HSE06. Moreover, the good performance of the SRhSG4 is also maintained for other test cases, except barrier heights (HTBH38 and NHTBH38) and charge transfer complexes (CT7).

TABLE VIII. MAEs (in kcal/mol) of the molecular benchmark tests obtained using various XC functionals. Best/worst MAE result of each test is shown in bold/underline style. The 6-311++G(3df,3pd) basis set was used. Total mean absolute error (TMAE) is given in the last row.

Test set	SG4	SRhSG4	HSEsol	HSE06
AE6 ^a	14.87	7.60	17.95	7.21
G2/148 ^b	<u>16.60</u>	7.25	19.37	7.04
EA13 ^c	4.47	2.77	2.81	2.78
IP13 ^d	3.03	<u>3.47</u>	2.39	3.21
PA8 ^e	1.54	1.35	1.27	<u>1.78</u>
HTBH38 ^f	<u>9.53</u>	4.88	6.79	3.48
NHTBH38 ^g	<u>8.27</u>	5.74	8.20	5.04
HB6 ^h	0.52	0.46	<u>0.95</u>	0.46
DI6 ⁱ	<u>0.53</u>	0.47	0.51	0.43
CT7 ^j	<u>3.08</u>	1.17	1.74	0.73
TMAE	<u>6.24</u>	3.52	6.20	3.22

^aSix atomization energies.

^batomization energies of 148 molecules.

^celectron affinity of 13 molecules.

^dionization potential of 13 molecules.

^e8 proton affinities.

^fhydrogen transfer barrier heights of 38 molecules,

^gnonhydrogen transfer barrier heights of 38 molecules.

^h6 hydrogen bonds.

ⁱ6 dipole interactions.

^j7 charge transfer complexes.

IV. CONCLUSIONS

To conclude, we have developed a screened range-separated hybrid functional (SRhSG4) by the satisfaction of the semiclassical atom theory through the modified gradient expansion of fourth-order (MGE4) and the local density linear response of the whole functional. We have assessed the SRhSG4 functional performance for equilibrium solid-state properties, structural phase transition of Si and Zr, ferroelectric properties of BaTiO₃ and PbTiO₃, band gaps of semiconductors, and optical absorption spectra of Si and C. Moreover, we have tested functional performance for the atomization energies, barrier heights, noncovalent interactions of molecules, and harmonium atom model system. Additionally, we have investigated the quality of the correlation potential obtained via the OEP method. It has been evinced that the constructed functional is more accurate than HSE06 for solid-state structural properties and much improved functional than HSEsol for the general purpose molecules. The improvement of the SRhSG4 over HSE06 and HSEsol is due to the satisfaction of the MGE4 and the LDA linear response criterion. The correlation potentials assessment, in turn, shows that all the HSE model-based functional can provide the correlation potentials reproducing most of the quantum oscillations of the high-level reference CCSD(T) counterpart.

The SRhSG4 performs in a more balanced way than HSEsol for both finite and extended systems. Thus, it may be a potential candidate to assess the various solid-state

applications. Moreover, the SRhSG4 can be used in the development of dielectric dependent range-separated hybrid density functionals [183,185,186].

We have studied only systems and properties where the dispersion interaction is not important. However, for layered materials and other van der Waals solids, as well as for interactions between molecules and surfaces, the SR hybrid functionals (HSE06, HSEsol, and SRhSG4) must include the nonlocal van der Waals correlation correction. In this sense, we recall that the GGA parents of these hybrid functionals have been already corrected for dispersion and weak interactions,

such as PBE+rVV10L [192], PBEsol+rVV10s [193,194], and SG4+rVV10m [194,195].

ACKNOWLEDGMENTS

S.J. is grateful to the NISER for partial financial support. S.Ś. is grateful to the Polish National Science Center for the partial financial support under Grant No. 2016/21/D/ST4/00903. VASP simulations has been performed on *KALINGA* and *NISERDFT* high-performance computing facility at NISER, Bhubaneswar.

-
- [1] W. Kohn and L. J. Sham, *Phys. Rev.* **140**, A1133 (1965).
- [2] P. Hohenberg and W. Kohn, *Phys. Rev.* **136**, B864 (1964).
- [3] G. E. Scuseria and V. N. Staroverov, in *Theory and Application of Computational Chemistry: The First 40 Years*, edited by C. E. Dykstra, G. Frenking, K. S. Kim, and G. E. Scuseria (Elsevier, Amsterdam, 2005), pp. 669–724.
- [4] F. Della Sala, E. Fabiano, and L. A. Constantin, *Int. J. Quantum Chem.* **22**, 1641 (2016).
- [5] A. Patra, S. Jana, L. A. Constantin, L. Chiodo, and P. Samal, *J. Chem. Phys.* **152**, 151101 (2020).
- [6] J. P. Perdew and K. Schmidt, *AIP Conf. Proc.* **577**, 1 (2001).
- [7] F. Tran, J. Stelzl, and P. Blaha, *J. Chem. Phys.* **144**, 204120 (2016).
- [8] L. Vega, J. Ruvireta, F. Vines, and F. Illas, *J. Chem. Theory Comput.* **14**, 395 (2017).
- [9] J. Sun, A. Ruzsinszky, and J. P. Perdew, *Phys. Rev. Lett.* **115**, 036402 (2015).
- [10] L. A. Constantin, E. Fabiano, J. M. Pitarke, and F. Della Sala, *Phys. Rev. B* **93**, 115127 (2016).
- [11] J. Tao and Y. Mo, *Phys. Rev. Lett.* **117**, 073001 (2016).
- [12] J. Tao, J. P. Perdew, V. N. Staroverov, and G. E. Scuseria, *Phys. Rev. Lett.* **91**, 146401 (2003).
- [13] B. Patra, S. Jana, L. A. Constantin, and P. Samal, *Phys. Rev. B* **100**, 155140 (2019).
- [14] B. Patra, S. Jana, L. A. Constantin, and P. Samal, *Phys. Rev. B* **100**, 045147 (2019).
- [15] J. Sun, J. P. Perdew, and A. Ruzsinszky, *Proc. Natl. Acad. Sci. USA* **112**, 685 (2015).
- [16] S. Jana, K. Sharma, and P. Samal, *J. Phys. Chem. A* **123**, 6356 (2019).
- [17] A. Patra, S. Jana, and P. Samal, *J. Phys. Chem. A* **123**, 10582 (2019).
- [18] A. Patra, S. Jana, H. Myneni, and P. Samal, *Phys. Chem. Chem. Phys.* **21**, 19639 (2019).
- [19] J. P. Perdew, J. Tao, V. N. Staroverov, and G. E. Scuseria, *J. Chem. Phys.* **120**, 6898 (2004).
- [20] S. Jana, L. A. Constantin, and P. Samal, *J. Chem. Theory Comput.* **16**, 974 (2020).
- [21] J. Sun, B. Xiao, Y. Fang, R. Haunschild, P. Hao, A. Ruzsinszky, G. I. Csonka, G. E. Scuseria, and J. P. Perdew, *Phys. Rev. Lett.* **111**, 106401 (2013).
- [22] Z.-h. Yang, H. Peng, J. Sun, and J. P. Perdew, *Phys. Rev. B* **93**, 205205 (2016).
- [23] J. P. Perdew, A. Ruzsinszky, G. I. Csonka, O. A. Vydrov, G. E. Scuseria, L. A. Constantin, X. Zhou, and K. Burke, *Phys. Rev. Lett.* **100**, 136406 (2008).
- [24] Y. Zhao and D. G. Truhlar, *J. Chem. Phys.* **128**, 184109 (2008).
- [25] Z. Wu and R. E. Cohen, *Phys. Rev. B* **73**, 235116 (2006).
- [26] A. E. Mattsson, R. Armiento, J. Paier, G. Kresse, J. M. Wills, and T. R. Mattsson, *J. Chem. Phys.* **128**, 084714 (2008).
- [27] A. E. Mattsson and R. Armiento, *Phys. Rev. B* **79**, 155101 (2009).
- [28] L. A. Constantin, A. Terentjevs, F. Della Sala, P. Cortona, and E. Fabiano, *Phys. Rev. B* **93**, 045126 (2016).
- [29] P. Elliott and K. Burke, *Can. J. Chem.* **87**, 1485 (2009).
- [30] P. Elliott, D. Lee, A. Cangi, and K. Burke, *Phys. Rev. Lett.* **100**, 256406 (2008).
- [31] M. Levy and J. P. Perdew, *Phys. Rev. A* **32**, 2010 (1985).
- [32] M. Levy, *Int. J. Quantum Chem.* **116**, 802 (2016).
- [33] J. P. Perdew and A. Zunger, *Phys. Rev. B* **23**, 5048 (1981).
- [34] P. Mori-Sánchez, A. J. Cohen, and W. Yang, *J. Chem. Phys.* **125**, 201102 (2006).
- [35] T. Tsuneda and K. Hirao, *J. Chem. Phys.* **140**, 18A513 (2014).
- [36] E. Fabiano and L. A. Constantin, *Phys. Rev. A* **87**, 012511 (2013).
- [37] S. Jana, B. Patra, H. Myneni, and P. Samal, *Chem. Phys. Lett.* **713**, 1 (2018).
- [38] V. U. Nazarov and G. Vignale, *Phys. Rev. Lett.* **107**, 216402 (2011).
- [39] J. Paier, M. Marsman, and G. Kresse, *Phys. Rev. B* **78**, 121201(R) (2008).
- [40] A. V. Terentjev, L. A. Constantin, and J. M. Pitarke, *Phys. Rev. B* **98**, 085123 (2018).
- [41] R. Garrick, A. Natan, T. Gould, and L. Kronik, *Phys. Rev. X* **10**, 021040 (2020).
- [42] J. Heyd, J. E. Peralta, G. E. Scuseria, and R. L. Martin, *J. Chem. Phys.* **123**, 174101 (2005).
- [43] J. Jaramillo, G. E. Scuseria, and M. Ernzerhof, *J. Chem. Phys.* **118**, 1068 (2003).
- [44] J. Heyd, G. E. Scuseria, and M. Ernzerhof, *J. Chem. Phys.* **118**, 8207 (2003).
- [45] J. Heyd and G. E. Scuseria, *J. Chem. Phys.* **121**, 1187 (2004).
- [46] B. Patra, S. Jana, and P. Samal, *Phys. Chem. Chem. Phys.* **20**, 8991 (2018).
- [47] S. Jana, A. Patra, and P. Samal, *J. Chem. Phys.* **149**, 094105 (2018).
- [48] S. Jana, A. Patra, L. A. Constantin, H. Myneni, and P. Samal, *Phys. Rev. A* **99**, 042515 (2019).

- [49] I. C. Gerber, J. G. Ángyán, M. Marsman, and G. Kresse, *J. Chem. Phys.* **127**, 054101 (2007).
- [50] B. G. Janesko, E. Proynov, G. Scalmani, and M. J. Frisch, *J. Chem. Phys.* **148**, 104112 (2018).
- [51] Y.-S. Lin, G.-D. Li, S.-P. Mao, and J.-D. Chai, *J. Chem. Theory Comput.* **9**, 263 (2013).
- [52] J.-D. Chai and M. Head-Gordon, *Phys. Chem. Chem. Phys.* **10**, 6615 (2008).
- [53] M. A. Rohrdanz, K. M. Martins, and J. M. Herbert, *J. Chem. Phys.* **130**, 054112 (2009).
- [54] J.-D. Chai and M. Head-Gordon, *J. Chem. Phys.* **128**, 084106 (2008).
- [55] O. A. Vydrov, J. Heyd, A. V. Krukau, and G. E. Scuseria, *J. Chem. Phys.* **125**, 074106 (2006).
- [56] T. M. Henderson, A. F. Izmaylov, G. Scalmani, and G. E. Scuseria, *J. Chem. Phys.* **131**, 044108 (2009).
- [57] J.-W. Song, S. Tokura, T. Sato, M. A. Watson, and K. Hirao, *J. Chem. Phys.* **127**, 154109 (2007).
- [58] E. Chermak, B. Mussard, J. G. Angyan, and P. Reinhardt, *Chem. Phys. Lett.* **550**, 162 (2012).
- [59] B. G. Janesko, T. M. Henderson, and G. E. Scuseria, *J. Chem. Phys.* **131**, 034110 (2009).
- [60] A. J. Garza, N. A. Wazzan, A. M. Asiri, and G. E. Scuseria, *J. Phys. Chem. A* **118**, 11787 (2014).
- [61] E. Weintraub, T. M. Henderson, and G. E. Scuseria, *J. Chem. Theory Comput.* **5**, 754 (2009).
- [62] G. I. Csonka, J. P. Perdew, and A. Ruzsinszky, *J. Chem. Theory Comput.* **6**, 3688 (2010).
- [63] E. Fabiano, L. A. Constantin, P. Cortona, and F. Della Sala, *J. Chem. Theory Comput.* **11**, 122 (2014).
- [64] R. Peverati and D. G. Truhlar, *J. Chem. Phys.* **135**, 191102 (2011).
- [65] H. S. Yu, X. He, S. L. Li, and D. G. Truhlar, *Chem. Sci.* **7**, 5032 (2016).
- [66] E. Fabiano, L. A. Constantin, and F. Della Sala, *Int. J. Quantum Chem.* **113**, 673 (2013).
- [67] J. Toulouse, I. C. Gerber, G. Jansen, A. Savin, and J. G. Ángyán, *Phys. Rev. Lett.* **102**, 096404 (2009).
- [68] J. Toulouse, F. Colonna, and A. Savin, *J. Chem. Phys.* **122**, 014110 (2005).
- [69] J. Toulouse and A. Savin, *J. Mol. Struct.* **762**, 147 (2006).
- [70] J. Toulouse, A. Savin, and H.-J. Flad, *Int. J. Quant. Chem.* **100**, 1047 (2004).
- [71] A. V. Krukau, G. E. Scuseria, J. P. Perdew, and A. Savin, *J. Chem. Phys.* **129**, 124103 (2008).
- [72] T. M. Henderson, B. G. Janesko, G. E. Scuseria, and A. Savin, *Int. J. Quant. Chem.* **109**, 2023 (2009).
- [73] J. Toulouse, P. Gori-Giorgi, and A. Savin, *Int. J. Quant. Chem.* **106**, 2026 (2006).
- [74] T. M. Henderson, A. F. Izmaylov, G. E. Scuseria, and A. Savin, *J. Chem. Phys.* **127**, 221103 (2007).
- [75] T. M. Henderson, A. F. Izmaylov, G. E. Scuseria, and A. Savin, *J. Chem. Theory Comput.* **4**, 1254 (2008).
- [76] F. Tran and P. Blaha, *Phys. Rev. B* **83**, 235118 (2011).
- [77] A. D. Becke and M. R. Roussel, *Phys. Rev. A* **39**, 3761 (1989).
- [78] T. M. Henderson, B. G. Janesko, and G. E. Scuseria, *J. Chem. Phys.* **128**, 194105 (2008).
- [79] M. Ernzerhof and J. P. Perdew, *J. Chem. Phys.* **109**, 3313 (1998).
- [80] L. Schimka, J. Harl, and G. Kresse, *J. Chem. Phys.* **134**, 024116 (2011).
- [81] S. Jana, A. Patra, L. A. Constantin, and P. Samal, *J. Chem. Phys.* **152**, 044111 (2020).
- [82] J. P. Perdew, K. Burke, and Y. Wang, *Phys. Rev. B* **54**, 16533 (1996).
- [83] E. Fabiano, L. A. Constantin, and F. Della Sala, *J. Chem. Phys.* **134**, 194112 (2011).
- [84] R. T. Sharp and G. K. Horton, *Phys. Rev.* **90**, 317 (1953).
- [85] J. D. Talman and W. F. Shadwick, *Phys. Rev. A* **14**, 36 (1976).
- [86] D. V. Feinblum, J. Kenison, and K. Burke, *J. Chem. Phys.* **141**, 241105 (2014).
- [87] E. H. Lieb and S. Oxford, *Int. J. Quant. Chem.* **19**, 427 (1981).
- [88] L. A. Constantin, A. Terentjev, F. Della Sala, and E. Fabiano, *Phys. Rev. B* **91**, 041120(R) (2015).
- [89] L. A. Constantin, J. C. Snyder, J. P. Perdew, and K. Burke, *J. Chem. Phys.* **133**, 241103 (2010).
- [90] L. A. Constantin, E. Fabiano, and F. Della Sala, *Phys. Rev. B* **84**, 233103 (2011).
- [91] L. A. Constantin, E. Fabiano, and F. Della Sala, *J. Chem. Phys.* **137**, 194105 (2012).
- [92] J. P. Perdew, M. Ernzerhof, and K. Burke, *J. Chem. Phys.* **105**, 9982 (1996).
- [93] A. V. Krukau, O. A. Vydrov, A. F. Izmaylov, and G. E. Scuseria, *J. Chem. Phys.* **125**, 224106 (2006).
- [94] P.-O. Widmark, P.-Å. Malmqvist, and B. O. Roos, *Theor. Chim. Acta* **77**, 291 (1990).
- [95] I. Grabowski, E. Fabiano, A. M. Teale, S. Śmiga, A. Buksztel, and F. Della Sala, *J. Chem. Phys.* **141**, 024113 (2014).
- [96] T. H. Dunning, *J. Chem. Phys.* **90**, 1007 (1989).
- [97] Q. Wu and W. Yang, *J. Chem. Phys.* **118**, 2498 (2003).
- [98] S. Śmiga and L. A. Constantin, *J. Phys. Chem. A* **124**, 5606 (2020).
- [99] S. Ivanov, S. Hirata, and R. J. Bartlett, *Phys. Rev. Lett.* **83**, 5455 (1999).
- [100] I. Grabowski and V. Lotrich, *Mol. Phys.* **103**, 2085 (2005).
- [101] E. Fabiano and F. Della Sala, *J. Chem. Phys.* **126**, 214102 (2007).
- [102] S. Śmiga, A. Buksztel, and I. Grabowski, in *Proceedings of the Electronic Structure Methods with Applications to Experimental Chemistry (MEST'12)*, edited by P. Hoggan, Advances in Quantum Chemistry (Academic Press, San Diego, 2014), Vol. 68, pp. 125–151.
- [103] E. Fabiano, S. Śmiga, S. Giarrusso, T. J. Daas, F. Della Sala, I. Grabowski, and P. Gori-Giorgi, *J. Chem. Theory Comput.* **15**, 1006 (2019).
- [104] S. Śmiga, S. Siecińska, and E. Fabiano, *Phys. Rev. B* **101**, 165144 (2020).
- [105] S. Śmiga and L. A. Constantin, *J. Chem. Theory Comput.* **16**, 4983 (2020).
- [106] S. Śmiga, O. Franck, B. Mussard, A. Buksztel, I. Grabowski, E. Luppi, and J. Toulouse, *J. Chem. Phys.* **145**, 144102 (2016).
- [107] S. Śmiga, I. Grabowski, M. Witkowski, B. Mussard, and J. Toulouse, *J. Chem. Theory Comput.* **16**, 211 (2020).
- [108] A. Buksztel, S. Śmiga, and I. Grabowski, in *Electron Correlation in Molecules—Ab initio Beyond Gaussian Quantum Chemistry*, edited by P. E. Hoggan and T. Ozdogan, Advances in Quantum Chemistry (Academic Press, San Diego, 2016), Vol. 73, pp. 263–283.

- [109] S. Śmiga, F. Della Sala, A. Buksztel, I. Grabowski, and E. Fabiano, *J. Comput. Chem.* **37**, 2081 (2016).
- [110] S. Śmiga, V. Marusiak, I. Grabowski, and E. Fabiano, *J. Chem. Phys.* **152**, 054109 (2020).
- [111] A. Görling, *Phys. Rev. Lett.* **83**, 5459 (1999).
- [112] I. Grabowski, A. M. Teale, S. Śmiga, and R. J. Bartlett, *J. Chem. Phys.* **135**, 114111 (2011).
- [113] K. Raghavachari, G. W. Trucks, J. A. Pople, and M. Head-Gordon, *Chem. Phys. Lett.* **157**, 479 (1989).
- [114] S. Śmiga, E. Fabiano, L. A. Constantin, and F. Della Sala, *J. Chem. Phys.* **146**, 064105 (2017).
- [115] S. Śmiga, L. A. Constantin, F. Della Sala, and E. Fabiano, *Computation* **7**, 65 (2019).
- [116] N. R. Kestner and O. Sinanoğlu, *Phys. Rev.* **128**, 2687 (1962).
- [117] C. Filippi, C. J. Umrigar, and M. Taut, *J. Chem. Phys.* **100**, 1290 (1994).
- [118] S. Kais, D. R. Herschbach, N. C. Handy, C. W. Murray, and G. J. Laming, *J. Chem. Phys.* **99**, 417 (1993).
- [119] E. Matito, J. Cioslowski, and S. F. Vyboishchikov, *Phys. Chem. Chem. Phys.* **12**, 6712 (2010).
- [120] C. Møller and M. S. Plesset, *Phys. Rev.* **36**, 618 (1934).
- [121] R. J. Bartlett, I. Grabowski, S. Hirata, and S. Ivanov, *J. Chem. Phys.* **122**, 034104 (2005).
- [122] G. Kresse and J. Hafner, *Phys. Rev. B* **47**, 558 (1993).
- [123] G. Kresse and J. Furthmüller, *Phys. Rev. B* **54**, 11169 (1996).
- [124] G. Kresse and D. Joubert, *Phys. Rev. B* **59**, 1758 (1999).
- [125] G. Kresse and J. Furthmüller, *Comput. Mater. Sci.* **6**, 15 (1996).
- [126] E. Aprà *et al.*, *J. Chem. Phys.* **152**, 184102 (2020).
- [127] J. Sun, M. Marsman, G. I. Csonka, A. Ruzsinszky, P. Hao, Y.-S. Kim, G. Kresse, and J. P. Perdew, *Phys. Rev. B* **84**, 035117 (2011).
- [128] A. B. Alchagirov, J. P. Perdew, J. C. Boettger, R. C. Albers, and C. Fiolhais, *Phys. Rev. B* **63**, 224115 (2001).
- [129] F. Gao, *Phys. Rev. B* **73**, 132104 (2006).
- [130] S. Jana, K. Sharma, and P. Samal, *J. Chem. Phys.* **149**, 164703 (2018).
- [131] P. Kovács, F. Tran, P. Blaha, and G. K. H. Madsen, *J. Chem. Phys.* **150**, 164119 (2019).
- [132] See Supplemental Material at <http://link.aps.org/supplemental/10.1103/PhysRevB.102.155107>, including Wilcoxon signed-rank test W values and the associated p values for lattice constants, bulk moduli, and cohesive energies of SG4, SRhSG4, HSEsol, and HSE06 functionals. Energy versus volume curve of different phases of Co and Ni as obtained from different methods are also supplied there.
- [133] A. J. Garza and G. E. Scuseria, *J. Phys. Chem. Lett.* **7**, 4165 (2016).
- [134] M. Ekholm, D. Gambino, H. J. M. Jönsson, F. Tasnádi, B. Alling, and I. A. Abrikosov, *Phys. Rev. B* **98**, 094413 (2018).
- [135] P. Söderlind and A. Gonis, *Phys. Rev. B* **82**, 033102 (2010).
- [136] Y. Fu and D. J. Singh, *Phys. Rev. B* **100**, 045126 (2019).
- [137] D. Mejía-Rodríguez and S. B. Trickey, *Phys. Rev. B* **100**, 041113(R) (2019).
- [138] L. Schimka, R. Gaudoin, J. Klimeš, M. Marsman, and G. Kresse, *Phys. Rev. B* **87**, 214102 (2013).
- [139] Y.-R. Jang and B.-D. Yu, *J. Magn.* **16**, 201 (2011).
- [140] B. Xiao, J. Sun, A. Ruzsinszky, J. Feng, R. Haunschild, G. E. Scuseria, and J. P. Perdew, *Phys. Rev. B* **88**, 184103 (2013).
- [141] R. G. Hennig, A. Wadehra, K. P. Driver, W. D. Parker, C. J. Umrigar, and J. W. Wilkins, *Phys. Rev. B* **82**, 014101 (2010).
- [142] R. Lizárraga, F. Pan, L. Bergqvist, E. Holmström, Z. Gercsi, and L. Vitos, *Sci. Rep.* **7**, 3778 (2017).
- [143] V. L. Moruzzi, P. M. Marcus, K. Schwarz, and P. Mohn, *Phys. Rev. B* **34**, 1784 (1986).
- [144] S. Jana, A. Patra, and P. Samal, *J. Chem. Phys.* **149**, 044120 (2018).
- [145] B. Xiao, J. Sun, A. Ruzsinszky, J. Feng, and J. P. Perdew, *Phys. Rev. B* **86**, 094109 (2012).
- [146] C. Shahi, J. Sun, and J. P. Perdew, *Phys. Rev. B* **97**, 094111 (2018).
- [147] T. M. Henderson, J. Paier, and G. E. Scuseria, *Phys. Status Solidi (b)* **248**, 767 (2011).
- [148] M. J. Lucero, T. M. Henderson, and G. E. Scuseria, *J. Phys.: Condens. Matter* **24**, 145504 (2012).
- [149] X.-D. Wen, R. L. Martin, T. M. Henderson, and G. E. Scuseria, *Chem. Rev.* **113**, 1063 (2013).
- [150] Y. Zhang, J. Sun, J. P. Perdew, and X. Wu, *Phys. Rev. B* **96**, 035143 (2017).
- [151] G. Shirane, H. Danner, and R. Pepinsky, *Phys. Rev.* **105**, 856 (1957).
- [152] H. H. Wieder, *Phys. Rev.* **99**, 1161 (1955).
- [153] K. M. Rabe, C. H. Ahn, and J.-M. Triscone, *Physics of Ferroelectrics: A Modern Perspective* (Springer, Berlin, 2007).
- [154] S. H. Wemple, *Phys. Rev. B* **2**, 2679 (1970).
- [155] D. I. Bilc, R. Orlando, R. Shaltaf, G.-M. Rignanese, J. Íñiguez, and P. Ghosez, *Phys. Rev. B* **77**, 165107 (2008).
- [156] G. Shirane, R. Pepinsky, and B. C. Frazer, *Acta Crystallogr.* **9**, 131 (1956).
- [157] J. Remeika and A. Glass, *Mater. Res. Bull.* **5**, 37 (1970).
- [158] K. Carl, *Ferroelectrics* **9**, 23 (1975).
- [159] B. Jaffe, W. R. Cook, and H. Jaffe, in *Piezoelectric Ceramics*, edited by B. JAFFE, W. R. Cook, and H. Jaffe (Academic Press, San Diego, 1971), pp. 115–134.
- [160] V. I. Zametin, *Phys. Status Solidi (b)* **124**, 625 (1984).
- [161] R. Wahl, D. Vogtenhuber, and G. Kresse, *Phys. Rev. B* **78**, 104116 (2008).
- [162] F. Corà, *Mol. Phys.* **103**, 2483 (2005).
- [163] T. Shimada, T. Ueda, J. Wang, and T. Kitamura, *Phys. Rev. B* **87**, 174111 (2013).
- [164] J. Sun, R. C. Remsing, Y. Zhang, Z. Sun, A. Ruzsinszky, H. Peng, Z. Yang, A. Paul, U. Waghmare, X. Wu, M. L. Klein, and J. P. Perdew, *Nat. Chem.* **8**, 831 (2016).
- [165] A. Paul, J. Sun, J. P. Perdew, and U. V. Waghmare, *Phys. Rev. B* **95**, 054111 (2017).
- [166] R. Peverati and D. G. Truhlar, *Philos. Trans. Roy. Soc. London A: Math. Phys. Eng. Sci.* **372**, 20120476 (2014).
- [167] A. J. Cohen, P. Mori-Sánchez, and W. Yang, *Science* **321**, 792 (2008).
- [168] A. J. Cohen, P. Mori-Sánchez, and W. Yang, *Chem. Rev.* **112**, 289 (2012).
- [169] P. Mori-Sánchez, A. J. Cohen, and W. Yang, *Phys. Rev. Lett.* **100**, 146401 (2008).
- [170] A. J. Cohen, P. Mori-Sánchez, and W. Yang, *Phys. Rev. B* **77**, 115123 (2008).
- [171] P. Mori-Sánchez, A. J. Cohen, and W. Yang, *Phys. Rev. Lett.* **102**, 066403 (2009).

- [172] J. P. Perdew, W. Yang, K. Burke, Z. Yang, E. K. U. Gross, M. Scheffler, G. E. Scuseria, T. M. Henderson, I. Y. Zhang, A. Ruzsinszky, H. Peng, J. Sun, E. Trushin, and A. Görling, *Proc. Natl. Acad. Sci. USA* **114**, 2801 (2017).
- [173] J. Tao, I. W. Bulik, and G. E. Scuseria, *Phys. Rev. B* **95**, 125115 (2017).
- [174] S. Jana and P. Samal, *Phys. Chem. Chem. Phys.* **20**, 8999 (2018).
- [175] D. Wing, J. B. Haber, R. Noff, B. Barker, D. A. Egger, A. Ramasubramaniam, S. G. Louie, J. B. Neaton, and L. Kronik, *Phys. Rev. Mater.* **3**, 064603 (2019).
- [176] M. Städele, M. Moukara, J. A. Majewski, P. Vogl, and A. Görling, *Phys. Rev. B* **59**, 10031 (1999).
- [177] M. Petersilka, U. J. Gossmann, and E. K. U. Gross, *Phys. Rev. Lett.* **76**, 1212 (1996).
- [178] Y.-H. Kim and A. Görling, *Phys. Rev. Lett.* **89**, 096402 (2002).
- [179] S. Sharma, J. K. Dewhurst, A. Sanna, and E. K. U. Gross, *Phys. Rev. Lett.* **107**, 186401 (2011).
- [180] S. Rigamonti, S. Botti, V. Veniard, C. Draxl, L. Reining, and F. Sottile, *Phys. Rev. Lett.* **114**, 146402 (2015).
- [181] M. Van Faassen, P. L. De Boeij, R. Van Leeuwen, J. A. Berger, and J. G. Snijders, *Phys. Rev. Lett.* **88**, 186401 (2002).
- [182] S. Cavo, J. A. Berger, and P. Romaniello, *Phys. Rev. B* **101**, 115109 (2020).
- [183] Y. Guo, J. Robertson, and S. J. Clark, *J. Phys.: Condens. Matter* **27**, 025501 (2014).
- [184] S. Refaely-Abramson, M. Jain, S. Sharifzadeh, J. B. Neaton, and L. Kronik, *Phys. Rev. B* **92**, 081204(R) (2015).
- [185] J. H. Skone, M. Govoni, and G. Galli, *Phys. Rev. B* **93**, 235106 (2016).
- [186] Z.-h. Yang, F. Sottile, and C. A. Ullrich, *Phys. Rev. B* **92**, 035202 (2015).
- [187] W. Chen, G. Miceli, G.-M. Rignanese, and A. Pasquarello, *Phys. Rev. Mater.* **2**, 073803 (2018).
- [188] N. P. Brawand, M. Govoni, M. Vörös, and G. Galli, *J. Chem. Theory Comput.* **13**, 3318 (2017).
- [189] N. P. Brawand, M. Vörös, M. Govoni, and G. Galli, *Phys. Rev. X* **6**, 041002 (2016).
- [190] A. T. Tal, P. Liu, G. Kresse, and A. Pasquarello, *Phys. Rev. Research* **2**, 032019 (2020).
- [191] C. Adamo and V. Barone, *J. Chem. Phys.* **110**, 6158 (1999).
- [192] H. Peng and J. P. Perdew, *Phys. Rev. B* **95**, 081105(R) (2017).
- [193] A. V. Terentjev, L. A. Constantin, and J. M. Pitarke, *Phys. Rev. B* **98**, 214108 (2018).
- [194] A. V. Terentjev, L. A. Constantin, E. Artacho, and J. M. Pitarke, *Phys. Rev. B* **100**, 235439 (2019).
- [195] A. Terentjev, P. Cortona, L. Constantin, J. Pitarke, F. Della Sala, and E. Fabiano, *Computation* **6**, 7 (2018).